Nanoscale Advances

PAPER

Check for updates

Nanozyme hydrogel for enhanced alkyl radical generation and potent antitumor therapy†

Shipeng Ning,‡[ac] Zeming Liu,‡[b] Mingzhu Chen, [iD] ‡[d] Daoming Zhu[e] and Qinqin Huang*[a]

Alkyl radicals (R•), which do not rely on oxygen generation for causing cellular stress, have been applied in tumor treatment, but a large amount of glutathione (GSH) in the tumor cells reacts with alkyl radicals, thereby reducing their antitumor effect. In this study, an enhanced alkyl radical generation system responsive to near-infrared light was designed. The alkyl radical trigger 2,2′-azobis[2-(2-imidazolin-2-yl) propane]-dihydrochloride (AIPH) and nanozyme pyrite (FeS_2) were encapsulated in agarose hydrogel to prepare the AIPH−FeS_2−hydrogel (AFH) system. FeS_2 can be used as a photothermal agent to convert near-infrared light energy into heat energy, leading to the dissolution of the hydrogel. AIPH is simultaneously induced to produce alkyl radicals. FeS_2 can also be used as an oxidative stress amplifier to reduce intracellular GSH content, thereby boosting the therapeutic effect of alkyl radicals. Eventually, the oxygen-independent free radicals generated by the AFH system under near-infrared laser irradiation and photothermal treatment can kill cancer cells through the synergistic oxidation/photothermal effect. The AFH system developed herein provides new insights into enhancing the therapeutic effect of alkyl radicals.

Introduction

In recent years, free radical-based treatments such as photodynamic therapy, sonodynamic therapy, and electrodynamic therapy have become popular choices for the treatment of breast cancer.[1–3] External stimuli (laser, ultrasound, electric fields) promote the production of reactive oxygen species (ROS) that induce cell death by causing severe oxidative damage or cell metabolism dysfunction.[4–6] Unfortunately, the hypoxic tumor environment and rapid tumor cell proliferation reduce the therapeutic outcomes of such treatments that rely on ROS production especially in the treatment of solid tumors.[7–10] Alkyl radicals are a new type of free radicals that do not depend on oxygen generation to kill cells and have been shown to be

effective in the treatment of tumors in normoxic and hypoxic environments.[11] The released alkyl radicals can induce apoptosis of cancer cells by increasing oxidative stress, leading to cellular lipid and DNA damage. As a typical free radical initiator, 2,2′-azobis[2-(2-imidazolin-2-yl)propane]-dihydrochloride (AIPH) can generate alkyl radicals at high temperatures.[12] It does so even in the absence of oxygen. The generated free radicals are toxic to cells and will immediately oxidize cell elements or interact with oxygen to produce secondary toxic substances.[13] Even in a hypoxic tumor microenvironment, AIPH can produce alkyl radicals to increase intracellular lipid hydroperoxide and further trigger tumor cell apoptosis.[14] All these indicate that R• is a promising cancer treatment drug.

Light or heat is used as an external stimulus in photothermal therapy.[15–17] Photothermal therapy (PTT) based on near-infrared (NIR) laser irradiation has been used to prevent tumor cell aggregation; it relies on local thermal effects to remove the tumors.[18–20] Several photothermal agents (PTAs) such as gold nanocrystals and molybdenum disulfide are used in combination with AIPH to release alkyl radicals in response to infrared laser irradiation.[19,21–23] However, the tumor microenvironment (TME) usually has a high level of glutathione (GSH) expression in solid tumors because GSH plays an important role in resisting radiotherapy through a spontaneous reaction or a GSH S-transferase catalyzed reaction with xenogenics.[24,25] In addition, as a reducing agent, GSH can directly remove alkyl radicals.[21,26] This reduces the effectiveness of alkyl radical-based therapies.

[a]The Research and Application Center of Precision Medicine, The Second Affiliated Hospital, Zhengzhou University, Zhengzhou, P.R.China. E-mail: qqhuang@zzu.edu.cn

[b]Department of Plastic Surgery, Tongji Hospital, Tongji Medical College, Huazhong University of Science and Technology, Wuhan 430030, China

[c]Department of Breast Surgery, Guangxi Medical University Cancer Hospital, Nanning, 530000, China

[d]Department of Radiation and Medical Oncology, Hubei Key Laboratory of Tumor Biological Behaviors, Hubei Cancer Clinical Study Center, Zhongnan Hospital of Wuhan University, Wuhan 430071, China

[e]Department of General Surgery & Guangdong Provincial Key Laboratory of Precision Medicine for Gastrointestinal Tumor, Nanfang Hospital, The First School of Clinical Medicine, Southern Medical University, Guangzhou, Guangdong, 510515, China

† Electronic supplementary information (ESI) available. See https://doi.org/10.1039/d2na00395c

‡ S. Ning, Z. Liu and M. Chen contributed equally to this work.

Pyrite (FeS_2) nano-enzyme, as a novel photothermal nanomaterial, not only has a good photothermal effect under NIR light but also has a nano-enzyme activity.[27] The FeS_2 nanase has demonstrated similar activity to glutathione oxidase (GSH-OXD), oxidizing GSH to oxidized glutathione (GSSG).[28] In the TME, GSH depletion was found to disrupt the REDOX balance of cells and cause oxidative stress.[29] Therefore, FeS_2 is expected to achieve a good synergistic effect with AIPH.

Minimally invasive photoresponsive hydrogels have recently become popular as a controlled drug release platform.[30–32] Hydrogels coagulate as they are injected into tumor tissue and serve as a long-term depot.[33] This topical form of administration can be repeated after a single injection. In addition, parameters such as laser power and irradiation time can be modified to change the drug release rate, thus extending the applicability of this treatment method.[34,35] Given these advantages, it was hypothesized that the use of hydrogels to deliver FeS_2 and AIPH to the TME would improve the efficacy of free radical-based therapies.

In this study, a method using intratumoral delivery of an injectable hydrogel containing FeS_2 nanozyme and the free radical initiator AIPH was designed. First, a hybrid system of AIPH-FeS_2-hydrogel (AFH) was prepared by loading FeS_2 nanoparticles and AIPH into agarose hydrogel. The hydrogel is solid at room temperature, and FeS_2 and AIPH are encapsulated within its matrix. Once irradiated by near-infrared (NIR) light, FeS_2 converts NIR light energy into heat energy, which causes the AFH system to heat up, and then the hydrogel melts and releases FeS_2 and AIPH. At high temperatures, AIPH decomposes to produce alkyl radicals. Subsequently, FeS_2 nanozyme, which mimics the activity of GSH-OXD, reduces the intracellular GSH content. The destruction of GSH will promote the killing effect of alkyl radicals. Because AFH can reside at the tumor site for a long time, the AFH system can allow precise control over the release of alkyl radicals by changing the laser intensity and radiation time. Finally, the oxygen-independent free radicals generated by the AFH system under NIR irradiation and photothermal treatment can synergistically kill cancer cells through the synergistic oxidation/photothermal effect, and tumor growth during the treatment cycle is well inhibited. In short, the AFH system designed herein further amplifies the therapeutic effect of AIPH by changing the redox homeostasis (Scheme 1).
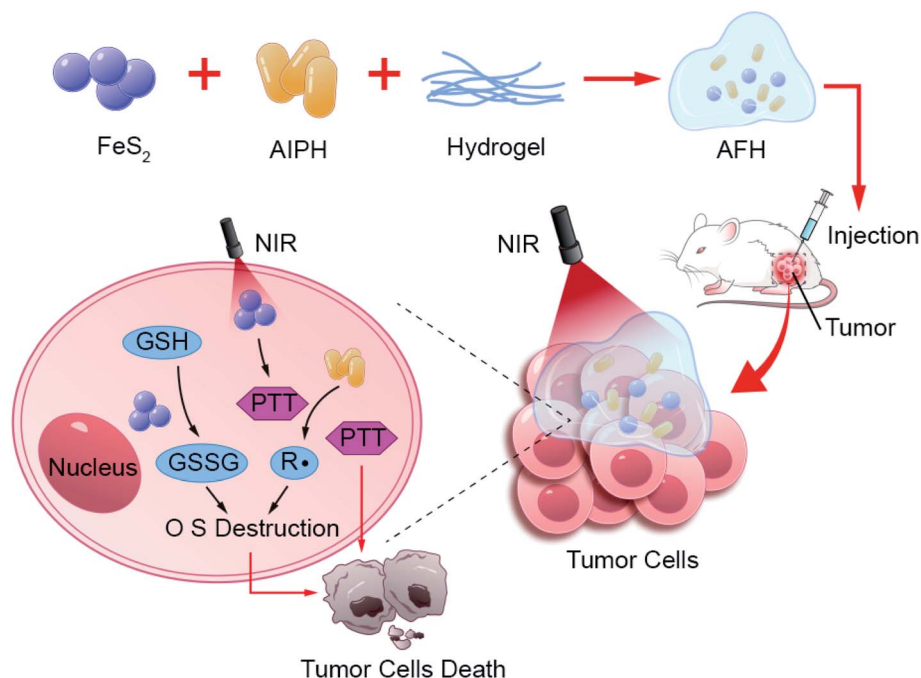
Results and discussion

A low-melting-point agarose hydrogel was used to prepare a composite hydrogel containing FeS_2 and AIPH. FeS_2 was mixed with an aqueous agarose solution at 60 °C and then loaded with the alkyl radical trigger AIPH, followed by quickly cooling to room temperature. Thus, the AFH hydrogel matrix was formed. Transmission electron microscopy was used to characterize the morphology of FeS_2 (Fig. 1A). The FeS_2 nanozyme showed sphere-like morphology with an average particle size of about 148 nm (Fig. S1†). The UV-vis absorption spectra of FeS_2 (Fig. 1B) showed that FeS_2 strongly absorbed in the NIR range at 808 nm. This property makes FeS_2 a good PTA. The photothermal performance of FeS_2 nanozyme at different

concentrations (0, 25, 50, and 100 μg mL^{-1}) was studied by irradiating the solution with a 0.5 W cm^{-2} 808 nm laser system (Fig. 1C). The heating effect of the solution was directly proportional to the FeS_2 concentration. The temperature of a 100 μg mL^{-1} FeS_2 solution increased by about 17.5 °C in just 5 min of laser irradiation, demonstrating the good photothermal performance of FeS_2. Scanning electron microscopy also showed that the AFH hydrogel has a complex network of pore structure and pore size distribution (Fig. 1D), which makes the hydrogel suitable for drug loading for delivery. Photothermal stability is also an important criterion for evaluating the quality of a PTA.[36] A 200 μg mL^{-1} FeS_2 solution was heated with an 808 nm NIR laser for 5 min, then the laser was turned off, and the FeS_2 solution was allowed to cool naturally to room temperature. This process was repeated several times to evaluate the photothermal stability of FeS_2 (Fig. 1E). There was no obvious change in the heating curve of each photothermal cycle, and only a slight difference was observed in the peak temperature achieved after 5 min of irradiation, verifying the photothermal stability of FeS_2. Rheological analysis also revealed a high storage modulus of the prepared hydrogel in the solid state at room temperature (Fig. 1F). As the temperature increased, the hydrogel gradually softened and dissolved, and the storage modulus gradually decreased. Next, a photothermal dissolution experiment was conducted on the FeS_2 hydrogel. The solidified AFH (FeS_2 contained in the hydrogel) was placed in a glass dish containing deionized water. At room temperature, the prepared AFH hydrogel maintained its solidified shape, but after 10 min of irradiation with an 808 nm laser, the hydrogel almost completely dissolved, and the FeS_2 nanomaterial was released and dissolved into the water in the glass dish (Fig. 1G). A thermal infrared imager also confirmed the significant increase in temperature of AFH during the irradiation (Fig. 1H). X-ray photoelectron spectroscopy (XPS) spectrum of FeS_2 after reaction with hydrogel showed that FeS_2 contained Fe and S elements (Fig. S2†). As shown in Fig. S3,† GSH content was significantly decreased after the co-incubation of FeS_2 and GSH, it has a positive correlation curve with time and concentration. Furthermore, the POD-like activity of the FeS_2 was size-dependent. Nanozymes with a size of 150 nm showed higher activity than those with sizes of 280 and 687 nm (Fig. S4†).

Based on the high-performance characteristics of AFH, its antitumor effects were evaluated. Initially, the fluorescein diacetate/propidium iodide live/dead cell staining kit was used to explore the killing effect of the prepared AFH hydrogel combined with NIR irradiation. The PBS + NIR group and the AFH only group showed strong green fluorescence, whereas AIPH hardly showed any killing effect (Fig. 2A). We prepared hydrogel only containing FeS_2 (FH) to verify relative experiments results. The prepared hydrogel containing only FeS_2 (FH) combined with NIR had a moderate killing effect. Notably, AFH + NIR treatment had the best cytotoxic effect.

The dichlorofluorescein diacetate probe was used to detect the ability of AIPH to produce ROS. AIPH showed a weaker ability to induce ROS in the absence of laser irradiation, while FH loaded with FeS_2 showed a moderate degree of ROS production after NIR irradiation (Fig. 2B). The bright green

Scheme 1 Nanozyme hydrogel for enhanced alkyl radical generation and potent antitumor therapy.

fluorescence observed in the AFH + NIR treatment group could be attributed to the release of FeS_2 and AIPH after laser irradiation (Fig. 2C). Furthermore, the groups of AIPH and AIPH + NIR showed very little green fluorescence (Fig. S5†). The CCK-8 assay also showed the same results. The cell viability of the AFH + NIR group was about 8.5%, which was significantly different
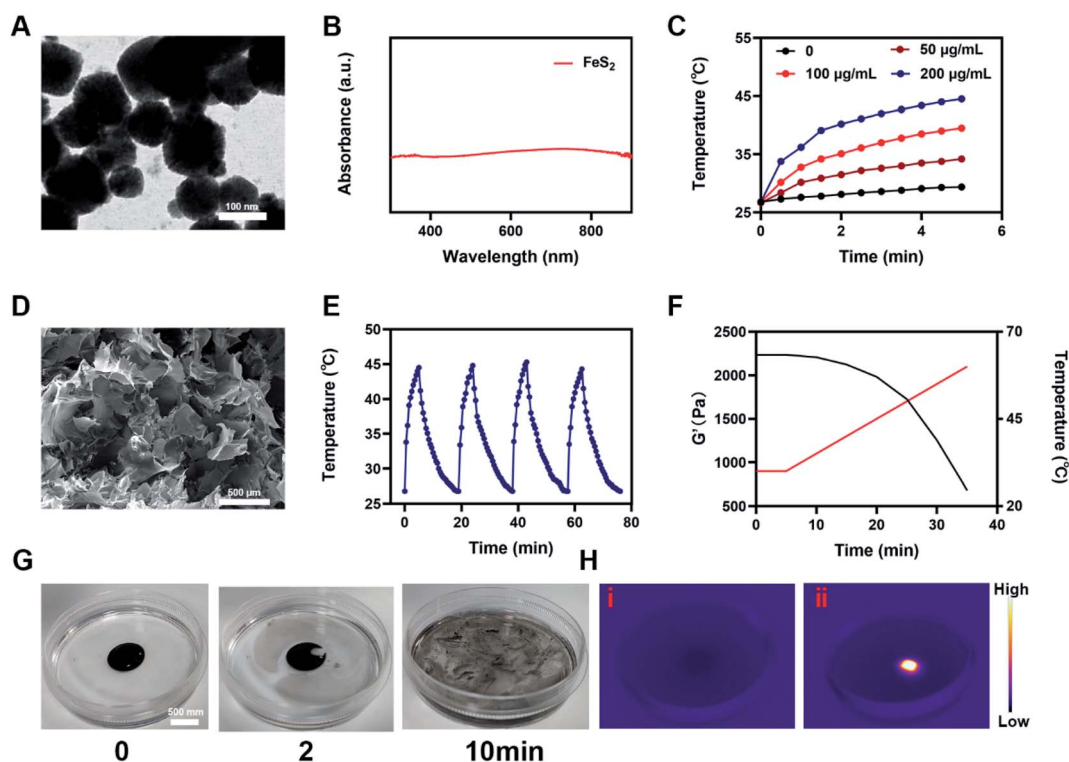

Fig. 1 (A) TEM image of FeS_2. (B) UV-Vis-NIR absorbance spectrum of a FeS_2 solution. (C) Heating curves for the different concentrations of FeS_2 nanoparticles solutions upon laser irradiation at 808 nm (0.5 W cm^{-2}) for 5 min. (D) SEM image of hydrogel. (E) Temperature variation of a FeS_2 solution under cyclic laser irradiation. (F) Rheological and temperature curves (red and black, respectively) for the prepared AFH in response to 0.5 W cm^{-2} 808 nm laser irradiation. (G) The morphology of the prepared AFH before and after 0.5 W cm^{-2} 808 nm laser irradiation for 10 min and (H) infrared thermal images of the prepared AFH following irradiation.
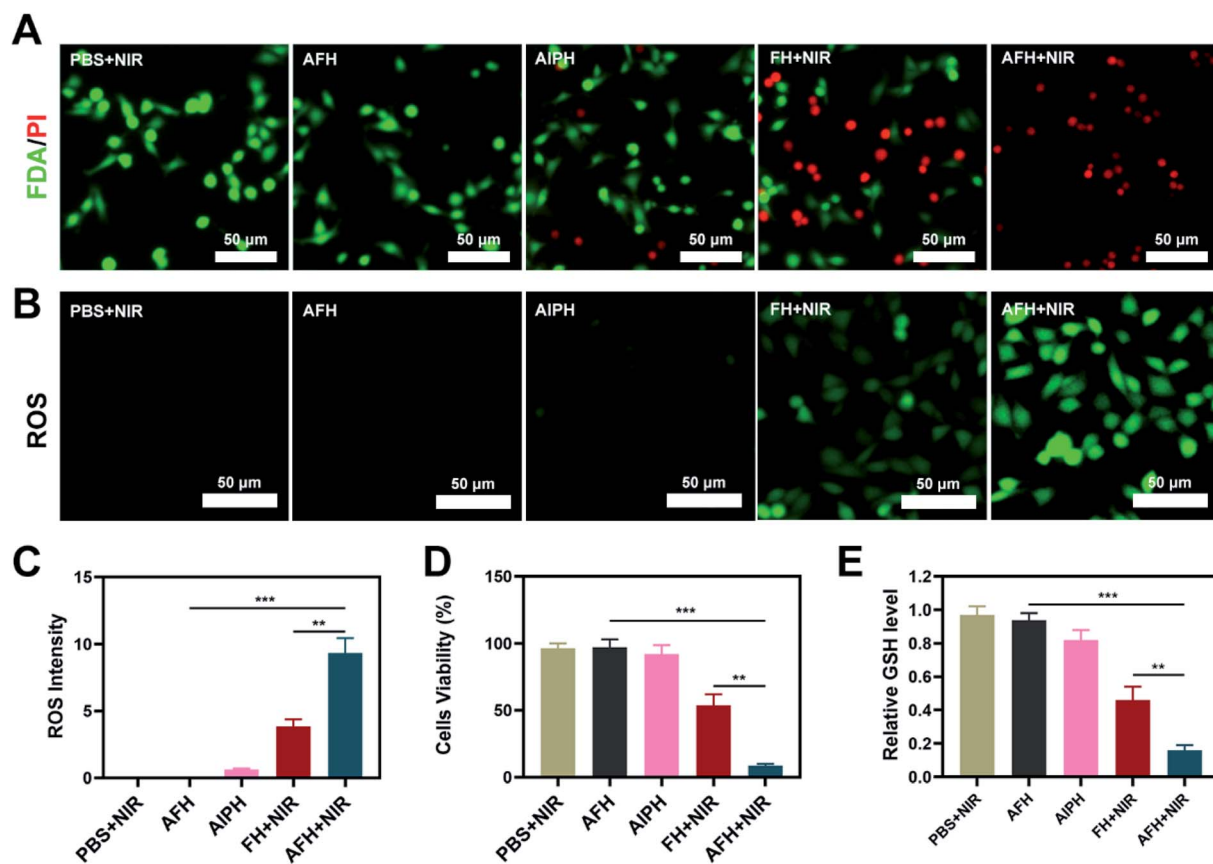
Fig. 2   (A) Fluorescence images of 4T1 cells stained with fluorescein diacetate (FDA) (live cells, green fluorescence) and propidium iodide (PI) (dead cells, red fluorescence) after incubation with different formulations. (B) Tumor cells DCFH–DA fluorescence images were observed after the indicated treatments. (C) DCFH–DA fluorescence intensity after the indicated treatments. (D) CCK-8 assays were conducted using 4T1 cells treated with different formulations. (E) Quantitative analysis of GSH levels with different formulations. $**P < 0.01$, $***P < 0.005$; Student's t-test.

from that of the other groups (Fig. 2D). High temperature will promote the decomposition of AIPH to produce alkyl radicals. At the same time, FeS_2 can exert GSH-OXD activity to reduce intracellular GSH. GSH, as a ubiquitous thiol-containing tripeptide, is synthesized from its constituent amino acids (glutamic acid, cysteine, and glycine) in many cells. GSH is produced abundantly in various types of cancer cells. GSH in cells generally exists in the reduced form, which can react with oxidizing substances such as alkyl groups while getting oxidized to its oxidized form glutathione disulfide (GSSG), thereby reducing the antitumor effect based on free radicals.[37] The depletion of GSH will disrupt the redox balance of cells, cause oxidative stress, and ultimately lead to cell apoptosis.[38] Ellman's reagent was used to test the ability of each group to deplete GSH. AFH combined NIR group showed the best GSH-depleting ability (Fig. 2E).

In view of its good *in vitro* performance as PTA and GSH-OXD-mimicking enzyme, the effect of AFH on the NIR light-to-heat conversion was studied *in vivo*. BALB/c mice were injected subcutaneously with 4T1 cells to form tumors. Fig. 3A shows the temperature change curve of the PBS group and the AFH group after 808 nm NIR laser 0.5 W cm^{-2} irradiation for 10 min. The temperature of the AFH group increased by about 17.6 °C

after the irradiation, while the temperature of the PBS group hardly increased. High temperature can change the fluidity of the tumor cell membrane, thereby increasing the permeability of the cell membrane, which in turn causes thermal damage to proteins.[39,40] Eventually, the cancer cells lose the ability to proliferate. Next, AFH-mediated antitumor activity was evaluated in 4T1 tumor-bearing mice. Tumor-bearing mice were divided randomly into five groups. The tumor volume of mice in the PBS + NIR group and AIPH group increased rapidly during the two-week treatment period, and the AFH group showed a slight tumor suppressor effect (Fig. 3C). This was because agarose was slowly metabolized, and some drugs were slowly released. The AFH + NIR group had the strongest effect on tumor growth. During the treatment, the tumor volume of the mice was significantly suppressed. After the treatment period, the mice were sacrificed, and the tumors were isolated and weighed. Results for tumor weight were consistent with results for tumor volume (Fig. 3D).

Importantly, during the entire study, no changes in body weight were observed in the treatment group, which indicates that the treatment did not cause any significant systemic toxicity to the mice (Fig. S6†). This result is very encouraging because although many materials have shown good
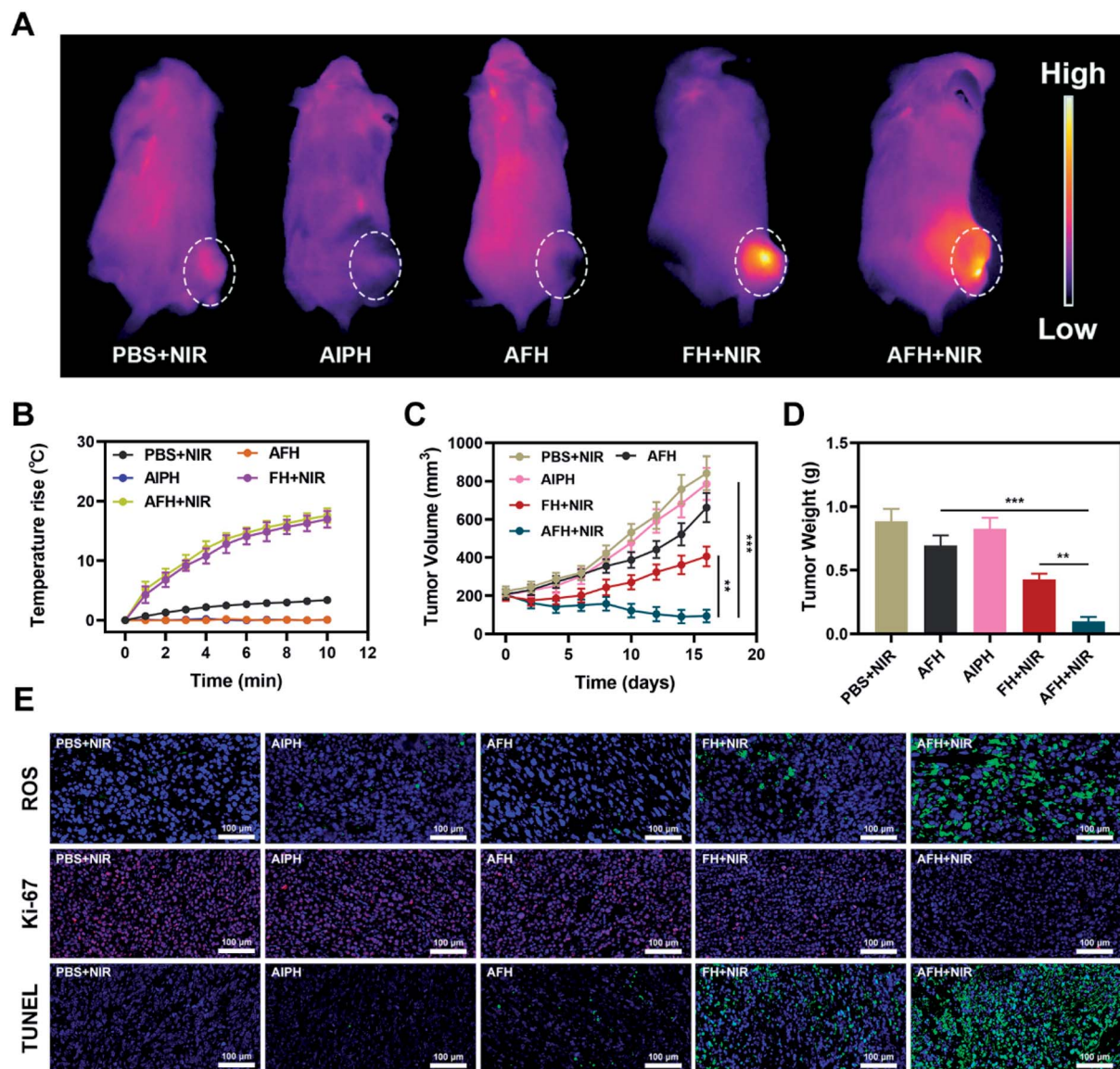
Fig. 3 (A) Infrared thermal images of tumors following irradiation with 808 nm laser (0.5 W cm^{-2}) for 10 min in the indicated treatment groups. (B) Temperature increases in mice implanted with 4T1 tumors following 808 nm laser irradiation (0.5 W cm^{-2}) for 10 min in the indicated treatment groups. (C) Tumor volume change over time in groups treated as indicated. (D) Average tumor weight values associated with the indicated treatments. (E) ROS, Ki-67 and TUNEL stained tumor sections from the indicated treatment groups. **$P < 0.01$, ***$P < 0.005$; Student's t-test.

experimental results, they also caused serious side effects, which seriously hinder their clinical prospects.[41,42] 2′,7′-Dichlorofluorescin diacetate was used to measure the intratumoral ROS generation in the treated mice. The staining was significantly enhanced in the tumors subjected to the combination therapy of AFH + NIR (Fig. 3E). The enhanced free radical production led to an enhanced therapeutic effect in the animal model. TUNEL and Ki-67 staining analyses were used to verify cell apoptosis and proliferation (Fig. 3E). Tumor tissues in the AFH + NIR group were massively necrotic without significant proliferation.

After treatment, the vital organs (heart, liver, spleen, lung, and kidney) did not have any inflammation or damage. The liver

and kidney indexes were normal (Fig. 4A–D and S7†). Comprehensive *in vivo* experimental data show that synergistic AFH and PTT therapy has good therapeutic effects and biocompatibility. It has good prospects for clinical medical applications in the future.

Conclusion

We designed an injectable photo-responsive hydrogel that can simultaneously achieve free radical therapy and PTT by encapsulating the nanozyme FeS$_2$ and the alkyl radical source AIPH into agarose hydrogel. Under 808 nm laser irradiation, the PTA FeS$_2$ promotes the heating of the AFH system and leads to the
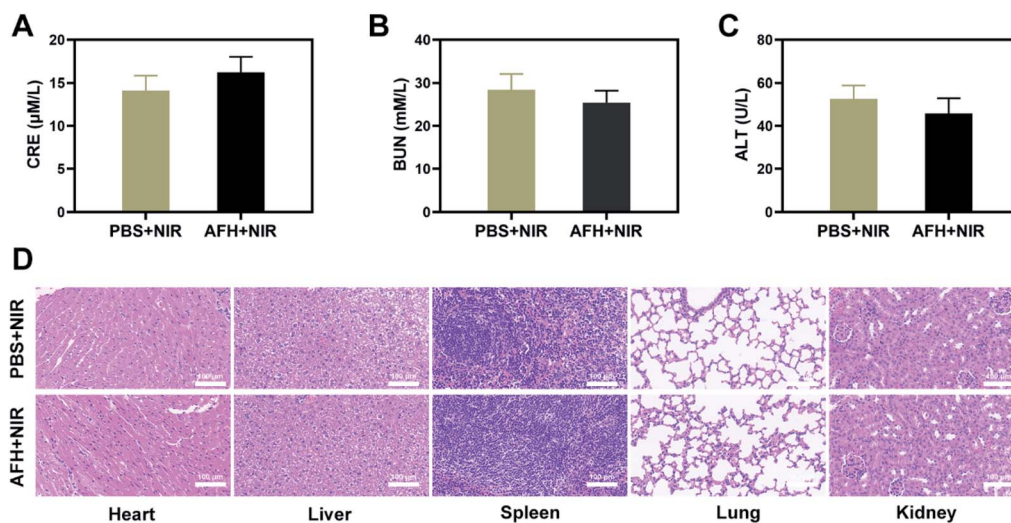
Fig. 4 Result of *in vivo* safety experiments. Blood biochemistry data including kidney function markers: (A) liver function markers: CRE, (B) BUN and (C) ALT after various treatments. (D) Histopathological analysis results (H&E-stained images) of the major organs, heart, lung, liver, kidneys, and spleen, of mice that were exposed to different treatments 16 days post-injection. Scale bars: 100 μm.

release of AIPH and its decomposition to produce alkyl radicals. At the same time, FeS_2 can reduce the intracellular GSH content, thereby further destroying the redox homeostasis. The dissolution rate of the hydrogel can be changed by parameters such as laser power density and spot size. Both *in vivo* and *in vitro* studies have shown that the combination of AFH with NIR irradiation can achieve powerful tumor-killing effects with insignificant adverse effects. The hydrogel system designed in this study provides a strategy to enhance therapeutic systems based on alkyl radicals.

Conflicts of interest

The authors declare that there are no conflicts of interest related to this article.

Acknowledgements

References

1 D. Zhu, J. Zhang, G. Luo, Y. Duo and B. Z. Tang, *Adv. Sci.*, 2021, e2004769.

2 C. Huang, S. Ding, W. Jiang and F.-B. Wang, *Nanoscale*, 2021, **13**, 4512–4518.

3 J. Wu, Y. Qu, K. Shi, B. Chu, Y. Jia, X. Xiao, Q. He and Z. Qian, *Chin. Chem. Lett.*, 2018, **29**, 1819–1823.

4 S. Ning, Y. Zheng, K. Qiao, G. Li, Q. Bai and S. Xu, *J. Nanobiotechnol.*, 2021, **19**, 344.

5 D. Zhu, T. Zhang, Y. Li, C. Huang, M. Suo, L. Xia, Y. Xu, G. Li and B. Z. Tang, *Biomaterials*, 2022, **283**, 121462.

6 D. Zhu, R. Ling, H. Chen, M. Lyu, H. Qian, K. Wu, G. Li and X. Wang, *Nano Res.*, 2022, DOI: **10.1007/s12274-022-4359-6**.

7 D. Zhu, M. Lyu, W. Jiang, M. Suo, Q. Huang and K. Li, *J. Mater. Chem. B*, 2020, **8**, 5312–5319.

8 H. Ranji-Burachaloo, P. A. Gurr, D. E. Dunstan and G. G. Qiao, *ACS Nano*, 2018, **12**, 11819–11837.

9 D. Zhu, Z. Liu, Y. Li, Q. Huang, L. Xia and K. Li, *Biomaterials*, 2021, **274**, 120894.

10 X. Li, R. Luo, X. Liang, Q. Wu and C. Gong, *Chin. Chem. Lett.*, 2021, DOI: **10.1016/j.cclet.2021.11.048**.

11 R. Xia, X. Zheng, X. Hu, S. Liu and Z. Xie, *ACS Appl. Mater. Interfaces*, 2019, **11**, 5782–5790.

12 W. Wu, Y. Yang, Z. Liang, X. Song, Y. Huang, L. Qiu, X. Qiu, S. Yu and W. Xue, *Nanoscale*, 2021, **13**, 11169–11187.

13 D. Cao, H. He, W. Li, J. Yan, J. Wu, M. Yin, Y. Zhou, Z. Zhou and L. Yin, *Biomater. Sci.*, 2021, **9**, 4054–4065.

14 S. Shen, C. Zhu, D. Huo, M. Yang, J. Xue and Y. Xia, *Angew. Chem.*, 2017, **56**, 8801–8804.

15 W. Liu, M. Ruan, Y. Wang, R. Song, X. Ji, J. Xu, J. Dai and W. Xue, *Small*, 2018, **14**, e1801754.

16 D. Zhu, M. Lyu, Q. Huang, M. Suo, Y. Liu, W. Jiang, Y. Duo and K. Fan, *ACS Appl. Mater. Interfaces*, 2020, **12**, 36928–36937.

17 D. Zhu, H. Chen, C. Huang, G. Li, X. Wang, W. Jiang and K. Fan, *Adv. Funct. Mater.*, 2022, 2110268.

18 Y. Qin, Q. Guo, S. Wu, C. Huang, Z. Zhang, L. Zhang, L. Zhang and D. Zhu, *Chin. Chem. Lett.*, 2020, **31**, 3121–3126.

19 K. Ding, C. Zheng, L. Sun, X. Liu, Y. Yin and L. Wang, *Chin. Chem. Lett.*, 2020, **31**, 1168–1172.

20 H. Wang, J. Yang, P. Cao, N. Guo, Y. Li, Y. Zhao, S. Zhou, R. Ouyang and Y. Miao, *Chin. Chem. Lett.*, 2020, **31**, 3015–3026.

21 J. Yang, R. Xie, L. Feng, B. Liu, R. Lv, C. Li, S. Gai, F. He, P. Yang and J. Lin, *ACS Nano*, 2019, **13**, 13144–13160.

22 H. Xiang, H. Lin, L. Yu and Y. Chen, *ACS Nano*, 2019, **13**, 2223–2235.

23 S. Wu, X. Liu, J. Ren and X. Qu, *Small*, 2019, **15**, 1904870.

24 W. Yin, J. Li, W. Ke, Z. Zha and Z. Ge, *ACS Appl. Mater. Interfaces*, 2017, **9**, 29538–29546.

25 Y. Wu, T. Guo, Y. Qiu, Y. Lin, Y. Yao, W. Lian, L. Lin, J. Song and H. Yang, *Chem. Sci.*, 2019, **10**, 7068–7075.

26 Y. Wan, G. Lu, J. Zhang, Z. Wang, X. Li, R. Chen, X. Cui, Z. Huang, Y. Xiao, J. Chelora, W. Zhang, Y. Liu, M. Li, H. Y. Xie and C. S. Lee, *Adv. Funct. Mater.*, 2019, **29**, DOI: **10.1002/adfm.201903436**.

27 D. She, S. Peng, L. Liu, H. Huang, Y. Zheng, Y. Lu, D. Geng and B. Yin, *Chem. Eng. J.*, 2020, **400**, DOI: **10.1016/j.cej.2020.125933**.

28 X. Meng, D. Li, L. Chen, H. He, Q. Wang, C. Hong, J. He, X. Gao, Y. Yang, B. Jiang, G. Nie, X. Yan, L. Gao and K. Fan, *ACS Nano*, 2021, DOI: **10.1021/acsnano.1c01248**.

29 P. Yu, X. Li, G. Cheng, X. Zhang, D. Wu, J. Chang and S. Wang, *Chin. Chem. Lett.*, 2021, **32**, 2127–2138.

30 C. Huang, B. Chen, M. Chen, W. Jiang and W. Liu, *Life*, 2021, **11**, DOI: **10.3390/life11050391**.

31 D. Zhu, Z. Zheng, G. Luo, M. Suo, X. Li, Y. Duo and B. Z. Tang, *Nano Today*, 2021, **37**, 101091.

32 M. Qiu, D. Wang, W. Liang, L. Liu, Y. Zhang, X. Chen, D. K. Sang, C. Xing, Z. Li, B. Dong, F. Xing, D. Fan, S. Bao, H. Zhang and Y. Cao, *Proc. Natl. Acad. Sci. U. S. A.*, 2018, **115**, 501–506.

33 M. Chen, Y. Tan, Z. Dong, J. Lu, X. Han, Q. Jin, W. Zhu, J. Shen, L. Cheng, Z. Liu and Q. Chen, *Nano Lett.*, 2020, DOI: **10.1021/acs.nanolett.0c02684**.

34 D. Chen, C. Chen, C. Huang, T. Chen and Z. Liu, *Front. Chem.*, 2020, **8**, 251.

35 H. Ma, C. He and X. Chen, *Macromol. Biosci.*, 2021, e2100039.

36 C. Cao, H. Zou, N. Yang, H. Li, Y. Cai, X. Song, J. Shao, P. Chen, X. Mou, W. Wang and X. Dong, *Adv. Mater.*, 2021, e2106996.

37 B. Niu, K. Liao, Y. Zhou, T. Wen, G. Quan, X. Pan and C. Wu, *Biomaterials*, 2021, **277**, 121110.

38 J.-S. Lan, L. Liu, R.-F. Zeng, Y.-H. Qin, J.-W. Hou, S.-S. Xie, S. Yue, J. Yang, R. J. Y. Ho, Y. Ding and T. Zhang, *Chem. Eng. J.*, 2021, **407**, DOI: **10.1016/j.cej.2020.127212**.

39 K. F. Chu and D. E. Dupuy, *Nat. Rev. Cancer*, 2014, **14**, 199–208.

40 C. Liu, J. Xing, O. U. Akakuru, L. Luo, S. Sun, R. Zou, Z. Yu, Q. Fang and A. Wu, *Nano Lett.*, 2019, **19**, 5674–5682.

41 Y. Zhu, H. Shi, T. Li, J. Yu, Z. Guo, J. Cheng and Y. Liu, *ACS Appl. Mater. Interfaces*, 2020, **12**, 18309–18318.

42 L. Jin, P. Hu, Y. Wang, L. Wu, K. Qin, H. Cheng, S. Wang, B. Pan, H. Xin, W. Zhang and X. Wang, *Adv. Mater.*, 2020, **32**, e1906050.